National Renewable Energy Laboratory
A national laboratory of the U.S. Department of Energy
Office of Energy Efficiency & Renewable Energy
Innovation for Our Energy Future

An Unlikely Combination of Experiments With a Novel High-Voltage CIGS Photovoltaic Array

Preprint

J.A. del Cueto and B.R. Sekulic

Presented at the 2006 IEEE 4th World Conference on Photovoltaic Energy Conversion (WCPEC-4)
Waikoloa, Hawaii
May 7–12, 2006

Conference Paper
NREL/CP-520-39877
May 2006

NREL is operated by Midwest Research Institute • Battelle Contract No. DE-AC36-99-GO10337

NOTICE

Available electronically at http://www.osti.gov/bridge

Available for a processing fee to U.S. Department of Energy and its contractors, in paper, from:

U.S. Department of Energy
Office of Scientific and Technical Information
P.O. Box 62
Oak Ridge, TN 37831-0062
phone: 865.576.8401
fax: 865.576.5728
email: mailto:reports@adonis.osti.gov

Available for sale to the public, in paper, from:

U.S. Department of Commerce
National Technical Information Service
5285 Port Royal Road
Springfield, VA 22161
phone: 800.553.6847
fax: 703.605.6900
email: orders@ntis.fedworld.gov
online ordering: http://www.ntis.gov/ordering.htm

Printed on paper containing at least 50% wastepaper, including 20% postconsumer waste

AN UNLIKELY COMBINATION OF EXPERIMENTS WITH A NOVEL HIGH-VOLTAGE CIGS PHOTOVOLTAIC ARRAY *

J.A. del Cueto, B.R. Sekulic
National Renewable Energy Laboratory (NREL), 1617 Cole Boulevard, Golden, CO 80401, USA

ABSTRACT

A new high-voltage array comprising bipolar strings of copper indium gallium diselenide (CIGS) photovoltaic (PV) modules was inaugurated in 2005. It is equipped with a unique combination of tests, which likely have never before been deployed simultaneously within a single array: full current-voltage (I-V) traces, high-voltage leakage current measurements, and peak-power tracking or temporal stepped-bias profiling. The array nominally produces 1 kW power at 1 sun. The array's electrical characteristics are continuously monitored and controlled with a programmable electronic load interfaced to a data acquisition system (DAS), that also records solar and meteorological data. The modules are mounted with their frames electrically isolated from earth ground, in order to facilitate measurement of the leakage currents that arise between the high voltage bias developed in the series-connected cells and modules and their mounting frames. Because the DAS can perform stepped biasing of the array as a function of time, synchronous detection of the leakage current data with alternating bias is available. Leakage current data and their dependence on temperature and voltage are investigated. Array power data are analyzed across a wide range of varying illuminations and temperatures from the I-V traces. Array performance is also analyzed from an energy output perspective using peak-power tracking data.

INTRODUCTION

A major goal of the U.S. Solar Program is the commercialization of PV modules with 30-year lifetimes or more, sustaining less than 0.5% annual performance degradation rate, and at costs consistent with market rates of electricity. To meet this goal, module reliability and performance stability need to be tested and insulated from stress mechanisms that precipitate module degradation—such as excessive exposure to moisture, temperature, and high voltage. In the 1980's, the Jet Propulsion Laboratory (JPL) investigated the connection between high-voltage leakage currents and contact corrosion in PV cells and modules, establishing key thresholds of accumulated charge—the cumulative integral of the leakage currents—that would result in 50% failures [1]. The thresholds for crystalline-silicon (c-Si) modules ranged 1–10 coulombs per centimeter length (C/cm) of module perimeter, and 0.1–1 C/cm for amorphous-silicon (a-Si) modules. At these thresholds, JPL found that the prime failure mechanism induced by high-voltage stress was electrochemical corrosion and degradation of the electrical contacts resulting in series-resistance increases. At NREL, we investigated high-voltage stress on c-Si and a-Si modules, and identified the dominant leakage current pathways as a function of temperature and humidity: conduction through the glass cover sheet at high relative humidity, and interface conduction under dry conditions [2]. In 2005, we installed a new CIGS PV array to investigate the effects of long-term exposure of this technology to high voltage stress and assess how well it can meet program goals.

EXPERIMENTAL PROCEDURE

The array comprises 24 thin-film CIGS modules deployed in two, bipolar strings of 12 modules connected in series, with nominally ±300 VDC open-circuit voltage and 1 kW total power. The modules are segregated into four groups of six modules, two groups for each string. Prior to deployment, all the modules were baseline tested at standard test conditions (STC). All the modules tested between 8.6% and 10.8% efficiency at STC. We performed both the dry and wet hi-pot tests to ascertain that the modules met the high-voltage leakage current criteria: the leakage currents were well below 1 micro-amp. We set up three separate measurement capabilities for the array: full current-voltage (I-V) traces, peak-power tracking and/or stepped bias loading, and high-voltage leakage current measurements. The array is deployed at fixed latitude tilt (~40°) with respect to horizontal, and mounted on a fiberglass structure, electrically isolated from earth ground with ceramic insulators. The module frames are electrically connected to each other on the support structure and then routed through a resistive network before connection to earth ground. Leakage currents driven by the high-voltage built up by the series-connected modules will pass to ground via the frames, and across the resistive network, where they are sensed by differential voltage inputs on a data-logger. The electrical characteristics and bias of each string are controlled with a dual-channel programmable electronic load (PEL), interfaced to a DAS. The DAS controls the PEL and executes the I-V traces, peak power tracking, and/or stepped-bias voltage loading on a regular schedule. Also, module temperatures in each string, and irradiance data, sensed by a pyranometer, plus other meteorological elements are monitored by the DAS.

ANALYSIS AND RESULTS

Analysis of the data is realized by: 1) integration of peak-power tracking and irradiance data with time, yielding daily energy outputs; 2) accumulation of all I-V trace records, statistically filtering for predominantly clear-sky conditions, followed by analysis and segregation into irradiance bins; and 3) integration of the leakage current data out through the module frames, resulting in accumulated daily leakage charge. We arrive at array efficiency quotients from two distinct angles: one is from the more usual I-V trace data representing power measurements from each string, divided by the incident power on each string (area of the string times the irradiance), and the second is from the ratio of the daily energy output from each string divided by the daily insolation energy (integral over time of the irradiance), yielding an effective efficiency (η_{EFF}) defined by Eq. 1, analogous to the realistic reporting conditions (RRC) efficiency previously reported [3]. The I-V trace data are further characterized by the usual power parameters: open-circuit voltage (Voc), short-circuit current (Isc), and fill factor (FF). We note the average efficiency at STC (η_{STC}) for the positive (+) and negative (-) strings of the array: respectively, 9.64% and 9.53%. The total aperture area for each string is 4.877 m^2, equally split between groups in the string. The total perimeter length for each group of six modules is 1.915 m.

$$\eta_{EFF} = \int_{Daily} P_{MAX} \cdot dt \Big/ [Area_{String} \cdot \int_{Daily} Irr \cdot dt] \qquad (1)$$

Performance and Stability Analysis

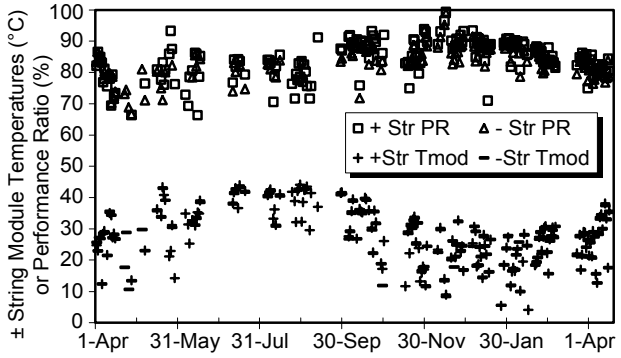

Fig. 1. Daily PR data and module temperatures for each of the ± strings, plotted against time starting April 2005.

In Fig. 1, we show the daily performance ratio (PR) data of the (+) and (-) strings of the array, derived from energy output analysis. The performance ratio are calculated as the ratio of the effective efficiency (η_{EFF}), derived by Eq. 1, divided by the average efficiency of all the modules in each of the respective strings as measured at STC (η_{STC}). In this graph, we also plot the average daytime module temperatures (Tmod) sampled from each of the strings. For convenience, we plot both PR and Tmod along the same abscissa, and note that the units of the PR are in %, while those of Tmod are °C. The data are plotted against time from April 2005 to April 2006. Figure 1 portrays the inverse dependence of the PR with average daytime module temperatures, ranging from 93%–99% in the winter down to about 70% in the summertime. We illustrate the usefulness of quantifying energy production performance via the PR with an example: on 13 April 2006, the integrated solar insolation was 8.53 kW-h/m^2, and the (+) and (-) strings attained 78.5% and 76.8% PR, respectively. So taking the product of the PR times the respective average η_{STC} and area for each string, times the insolation yields the energy output for each string, respectively, 3.14 and 3.05 kW-h.

We now present the array data derived from power analysis of the full I-V traces executed by the PEL and DAS, across varying illumination and temperatures. In Fig. 2, we depict the Voc and FF data reduced into irradiance bins 50W/m^2 wide and corrected to reference module temperature (25°C), plotted against irradiance, for each string. From Fig. 2, we observe that Voc for the (+) string is larger by ~3–5 volts than for the (-) string, and that for both, Voc goes from 285–290 volts at high irradiance, and drops down to ~225 volts at 50 W/m^2 irradiance. The FF data for both strings appear to be 59%–61% at high irradiance. Going from high irradiance down to 300 W/m^2, the FF for both strings increase by ~2% absolute. This increasing dependence of the FF with decreasing irradiance is consistent with series-resistance limited PV performance and is observed for single modules as well [4]. Below 300 W/m^2, the FF data diminish for both strings down to ~57%. Our capability to measure the array's full I-V characteristics enables us to dissect and identify potential failure modes in future deterioration of performance to greater degree than from mere optimum-power point data.

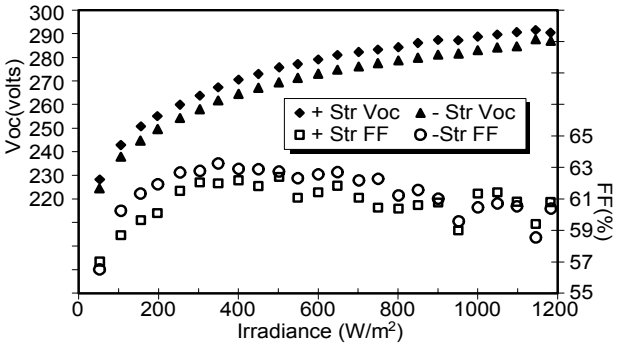

Fig. 2. Array Voc and FF for both strings corrected to 25°C module temperatures, respectively, read from left- and right-hand abscissae, plotted against irradiance.

In Fig. 3, we depict the efficiency data of each string plotted versus time, derived from power analysis of the full I-V traces executed by DAS and corrected to reference (25°C) module temperature, for a random sampling of cases with irradiance values within a window of 1000 ± 50 W/m^2. These data represent string power conversion efficiency taken under predominantly clear-sky conditions. The data for the (+) and (-) strings are read, respectively, along the left- and right-hand abscissae. The temperature coefficients of the efficiency (derived from power analysis)

were calculated piecewise in irradiance bins 50 W/m^2 wide, by linear regression against module temperatures: above 750 W/m^2 irradiance, these coefficients are an average of –0.19%/°C and –0.26%/°C, respectively, for the (+) and (-) strings, with 1 standard deviation of ~0.04%/°C. Fig. 3 shows that the average (+) string efficiency is about 9.1%, and just below that, 8.9%, for the (-) string. When we perform linear regression of the efficiency versus time for these data, we obtain no statistically significant degradation of performance from either string: the losses per year are at or less than 1 part in 10^3, and are about the same size as the statistical error in the coefficients.

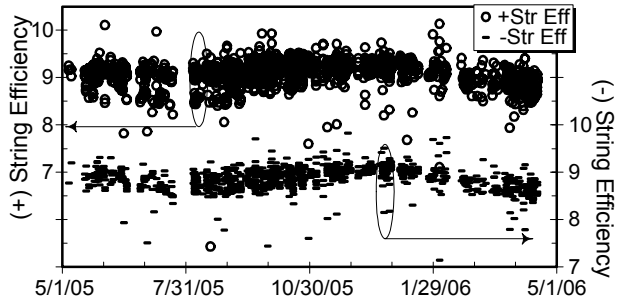

Fig. 3. Temperature-corrected array efficiency data at 1000 W/m^2, plotted versus time, for the (+) and (-) strings, respectively, read from left- and right-hand abscissae.

High-Voltage Leakage Currents

Previously, we had [2] analyzed the leakage currents from modules exposed to high-voltage stress and concluded that: leakage occurs along different pathways depending on the temperature and relative humidity, and is thermally activated with an activation energy that depends on humidity. In Fig. 4, we present the daily integrated leakage charge, expressed in milliCoulombs (mC), from each of the four groups of modules in the array portrayed on a semilog plot against the inverse of the average daily absolute module temperatures. For clarity, we've restricted the data to show only those corresponding to days where the energy out from each string was at or over 2.1 kW-h.

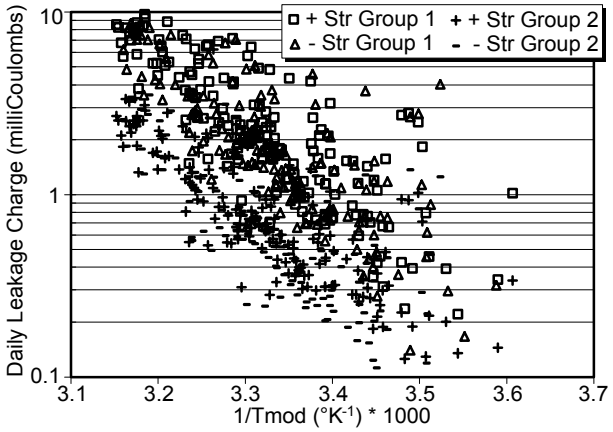

Fig. 4. Integrated daily leakage charge plotted against inverse absolute module temperature for each of the four module groups in the array.

We emphasize that each leakage charge datum depicted in Fig. 4 represents the combined leakage from the six modules all from within the same group. Because all the modules are connected in series, for the groups biased furthest from ground potential, the average cumulative bias on that group will be offset to its largest positive or negative value. These high-voltage groups are labeled as group 1 for both (+) and (-) strings in Fig. 4, while the groups of six modules with lower average bias are labeled as group 2. This is the reason that the leakage currents and charge for both group-1 modules in each string are about a factor of 2.8 to 2.9 larger than those of the group-2 modules—namely, it reflects the nearly linear partition of the string voltages across each module in each group and the fairly ohmic dependence of the leakage currents with bias. Aside from variations in leakage due to bias-dependence as discussed, there is significant scatter within each group's leakage data, which is predominantly due to the leakage dependence on humidity that is unaccounted for and is convoluted in the daily average data.

The thermally activated behavior of the charge leaked by the modules emanating from high-voltage bias is made evident in Fig. 4. From the slope of the characteristic exponential thermal dependence shown, one can derive the activation energy of the leakage charge for the data shown: the activation energies are 0.72 electron volts (eV), 0.64 eV, 0.78 eV, and 0.71 eV, respectively, for each of the string groups—(+) group 1, (+) group 2, and (-) group 1, (-) group 2—with a standard deviation of ~0.05 eV. The sizes of all the activation energies of the leaked charge strongly suggest that the leakage currents are dominated by conduction through the soda-lime silicate glass, whose electrical conductivity is thermally activated with activation energies between 0.6 and 0.8 eV [2, 5].

At this stage, it is worthwhile to estimate the potential lifetime crisis point emanating from high-voltage stress for these modules by using the data in Fig. 4, and by recalling the damage threshold of accumulated charge—resulting in 50% failure rate, as determined by JPL—was on the order of 0.1–1 Coulombs per centimeter of perimeter (C/cm) for a-Si thin-film modules. Although there is no guarantee that those damage thresholds are strictly applicable to the CIGS modules, it is still worthwhile to compare them with a-Si because of the similar encapsulation and thin-film construction of the devices. For the hottest days depicted in Fig. 4, the daily leakage charge for the higher-offset biased modules is 10 mC, which occurs when the average daytime module and air temperatures are, respectively, in the ranges of 40°–45°C and 23°–30°C. Although we don't get too many days like that in Colorado, days with similar or even hotter (~40°C) average daytime temperatures are common throughout the world. So we take the case of 10 mC leakage charge occurring on 200 days out of the year: over the course of 10 years, similar modules exposed to high voltage as the group 1 modules will accumulate 20 C of charge, that when spread evenly over 1.915 m of module perimeter, yields ~0.1 C/cm—which is significantly close to the lower threshold for damage determined by JPL. Hence, the exposure of this CIGS technology to high-voltage stress in hot climates merits further scrutiny.

We scrutinize the response of the leakage currents to changes in bias voltage. We portray this response in Fig. 5, which is a composite graph depicting the leakage currents—from the two higher offset bias groups in the array (± string groups 1)—on two different days, 18 April 2006 and 14 March 2006, respectively, at top and bottom portions of the graph, plotted against time of day. The corresponding string bias voltages vs. time are also shown in this graph and are read from the left-hand abscissae. The ± group-1 leakage currents are read along the right-hand abscissae. On these two days, the array was controlled in distinctly different modes: 1) tracking the optimum-power point (P_{OPP}) on Apr. 18 at top, and 2) in discreet voltage steps vs. time profile on Mar. 14 at bottom. The stepped-voltage vs. time profiles are executed with the PEL controlling the array in constant-voltage mode, while the DAS sends varying voltage setpoints vs. time to the PEL. Then, the bias the array actually develops is whatever it can deliver given the incident irradiance, either up to the setpoint or Voc, whichever one is less.

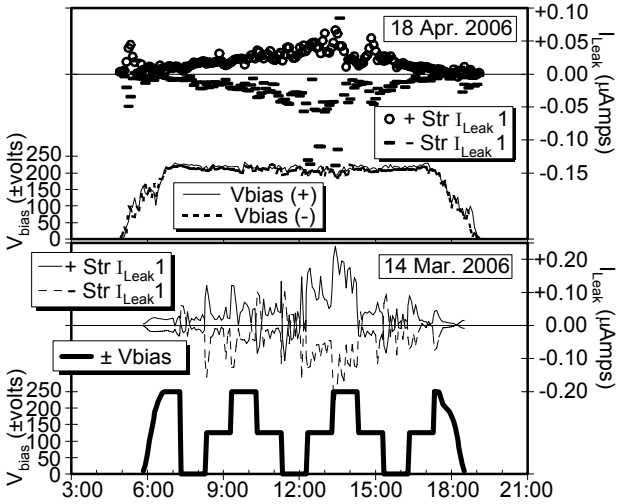

Fig. 5. Array bias and leakage currents vs. time profiles on two different days, with the array controlled in distinct ways: optimum power at top, or in discreet voltage steps bottom. Bias voltages and leakage currents are read, respectively, from left-hand or right-hand abscissae.

Note that when controlling the array in P_{OPP} mode, the bias voltages vs. time profiles are smooth, going from zero up to about ±210 volts for most of the day, and both strings' leakage currents exhibit smoothly varying behavior, obtaining maximum values, typically 0.05 to 0.1 microamps, in the early afternoon when the temperatures are at their highest. In contrast, when stepping the array bias in large fixed increments, the leakage currents appear to be larger by a factor two immediately after the bias is stepped, when incrementing to high voltage. Interestingly, when decrementing the bias in large discreet steps at bottom, the leakage currents actually flip to opposite polarity: the positive string leaks negative current, and the negative string vice-versa, for intervals that last on the order of minutes. Because there is no power supply in this circuit, other than the array itself, which is incapable of switching to net opposite polarity, one of the few ways this may be explained seems via a relaxation of a dipole layer of ion charges induced in the soda-lime glass adjacent to and by the high-voltage bias of the PV cells.

CONCLUSIONS

We have deployed a new array with unique capabilities: peak-power tracking, full I-V characteristic traces, and leakage current measurements, using CIGS thin-film PV modules in a high-voltage configuration. We have scrutinized array performance in two ways: from the I-V traces and energy output considerations. We present this performance in Table 1 below, derived both ways, with the caveat that we may not be weighing all days equally throughout the year due to array downtime. We emphasize the significance of the energy-based efficiency and performance ratio (PR) products in the 2nd and 4th rows: given an energy budget—like 6.1 kW-h/m^2/day—and when the average daytime air temperatures are 13°–14°C, the array will deliver 8.1% or 7.95% of this as electrical energy, respectively, from (+) and (-) strings. We give the energy-based relative temperature coefficient: –0.38%/°C versus average daytime air temperature. Note that the energy-based efficiencies are less than those derived at one irradiance and temperature listed in rows 3 and 5.

Table 1. Array performance.

String	Average Daytime Air Temp.	Average Module Temp.	Irradiance or Insolation	Eff (%) Method	PR (%)
+	14 °C	28 °C	6.12 kW-h/m^2/day	8.12 Energy	84.3
+	Temp. Corrected	25 °C	1001.5 W/m^2	9.11 Power	94.5
-	13 °C	27 °C	6.18 kW-h/m^2/day	7.95 Energy	83.5
-	Temp. Corrected	25 °C	1001.4 W/m^2	8.87 Power	93.1

ACKNOWLEDGEMENTS

This work was supported by the U.S. Department of Energy under Contract No. DE-AC36-99GO10337.

REFERENCES

[1] GR Mon, RG Ross. "Electrochemical Degradation of Amorphous-Silicon Photovoltaic Modules", *Proc. 18th IEEE PVSC*, Las Vegas, NV, p. 1142 (1985).

[2] JA del Cueto, T.J. McMahon, "Analysis of Leakage Currents in Photovoltaic Modules Under High Voltage Bias in the Field", *Progress in PV: Research & Applications* **10**, 15–28 (2002).

[3] K Bucher, G Kleiss, D Batzner, "RRC Module Energy Rating: A Module Survey", *Proc. 26th IEEE PVSC*, pp. 1187–1191 (1997).

[4] JA del Cueto, "Review of the Field Performance of One Cadmium Telluride Module", *Progress in PV: Research & Applications* **6**, 433-446 (1998).

[5] FV Tooley (ed.) *Handbook of Glass Manufacture*, Vol. II, Section 17: Physical Properties of Glass, Ashlee Pub. Co., New York, NY, 3rd edn. 1984, pp. 937–947.